Range of Ar, Kr, and Xe Ions in Solids in the 500-keV to 2-MeV Energy Region*

D. POWERS, W. K. CHU, AND P. D. BOURLAND
Baylor University, Waco, Texas
(Received 7 July 1967)

The range of Ar in Be and C, of Kr in Be, C, and Al, and of Xe in Be, C, and Al has been measured in 100-keV steps from 500 keV to 2 MeV with an accuracy varying from ±10.1 to 3.2%. The range of Xe in V, Ni, and Cu has been measured in 250-keV steps from 500 keV to 1.75 MeV with an accuracy of ±11.4 to 5.7%. Seven of the 11 sets of measurements agree to within 9% of the theory due to Lindhard, Scharff, and Schiøtt, with the best agreement in the energy region where electronic stopping is roughly equal to nuclear stopping. The measurements on Ar in Be and C are lower than the theory by 10–18% until a shell-structure correction of Ormrod, MacDonald, and Duckworth is applied, and then excellent agreement is obtained. The measurements on Xe in Ni and Cu are lower than the theory by 8–24%. Proton-stopping cross sections in V at 559, 1776, and 1984 keV are reported.

I. INTRODUCTION

IN 1948, Bohr[1] laid the foundation for a theoretical description of the energy loss of heavy ions of low velocity in matter. His analysis of the stopping process was then extended by Nielsen[2] and later by Lindhard and Scharff.[3] Nielsen's theory applied only to stopping of extremely low-velocity ions where the stopping process consisted entirely of elastic nuclear collisions, and where the interaction was by means of a $1/r^2$ potential. Lindhard and Scharff's work treated the nuclear elastic collisions through a Thomas-Fermi potential and also included an electronic-excitation contribution to the stopping which was to vary as the first power of the ion's velocity. More recently, Lindhard and co-workers[4] have given a detailed description of the stopping process in the velocity region $0<v<v_0Z_1^{2/3}$, where $v_0=e^2/\hbar$ and Z_1 is the atomic number of the incident ion. This theory by Lindhard and co-workers is applicable to polycrystalline solids or gaseous media.

In 1962, Powers and Whaling[5] measured the ranges of several ions in several solid targets in the energy region 50–500 keV. Their results, applicable to a random distribution of stopping atoms, indicated good agreement between theory and experiment. The purpose of the present experiment is to extend those measurements to the energy region 500 keV to 2 MeV in an attempt to make a systematic test of the theory.

II. EXPERIMENTAL METHOD

The experimental technique consists of the bombardment of highly polished metal targets by singly charged heavy ions, and then using the elastic scattering of protons from the target-plus-embedded-atom medium to determine the penetration depth. Figure 1 gives a diagram of the experimental arrangement. Singly charged heavy ions of Xe, Kr, and Ar are produced in the rf ion source of the Baylor 2-MeV Van de Graaff accelerator. The ions are focused with the strong-focusing quadrupole magnet and are analyzed in a 20° magnetic analyzer which holds the beam energy monoenergetic to within 0.15%. The analyzer is able to resolve isotopes in the Kr and Xe beam, but the beam is diffused with the quadrupole magnet and is trimmed with collimators to provide a spot of approximately uniform intensity and of size $\frac{1}{8}$ in.$\times\frac{1}{8}$ in. on the target. The normal isotopic composition of the beam is assumed throughout the measurements. The magnetic analyzer is calibrated against the $F^{19}(p, \alpha\gamma)$ resonance at 872.1 keV.[6] Separate calibrations using $Li^7(p, n)$ at 1880.6 keV,[6] $Li^7(p, \gamma)$ at 441.2 keV,[7] $F^{19}(p, \alpha\gamma)$ at 1346.6[7] and at 1373.5 keV[7] indicate that the magnetic analyzer is linear to within 0.15% over the energy region 0.4–1.9 MeV. The magnetic analyzer was periodically calibrated throughout all the measurements reported in this paper. The ion-beam current density varied from about 1–5 μA/cm^2, with the beam current usually being of the order of 0.2 μA (2μA/cm^2). The total charge deposited was 900 μC/cm^2 for Xe^+, 5000 μC/cm^2 for Kr^+, and approximately 9000 μC/cm^2 for Ar^+.

After bombardment of the target with heavy ions, a proton beam was obtained from the accelerator and was trimmed and collimated to a small spot (approximately 1 mm×1 mm). The beam was directed so as to strike a portion of the spot previously bombarded by the heavy ions. The proton scattering normally immediately followed the heavy-ion bombardment, although occasionally the proton bombardment would be delayed by several hours. No detectable diffusion of the ion in the target was observed, since the same

* Research supported in part by the National Science Foundation.
[1] N. Bohr, Kgl. Danske Videnskab. Selskab, Mat. Fys. Medd. **18**, No. 8 (1948).
[2] K. O. Nielsen, in *Electromagnetically Enriched Isotopes and Mass Spectrometry*, edited by M. L. Smith (Academic Press Inc., New York, 1956), p. 68.
[3] J. Lindhard and M. Scharff, Phys. Rev. **124**, 128 (1961).
[4] J. Lindhard, M. Scharff, and H. E. Schiøtt, Kgl. Danske Videnskab. Selskab, Mat. Fys. Medd. **33**, No. 14 (1963).
[5] D. Powers and W. Whaling, Phys. Rev. **126**, 61 (1962).
[6] J. B. Marion, Rev. Mod. Phys. **38**, 660 (1966).
[7] J. B. Marion, Rev. Mod. Phys. **33**, 139 (1961).

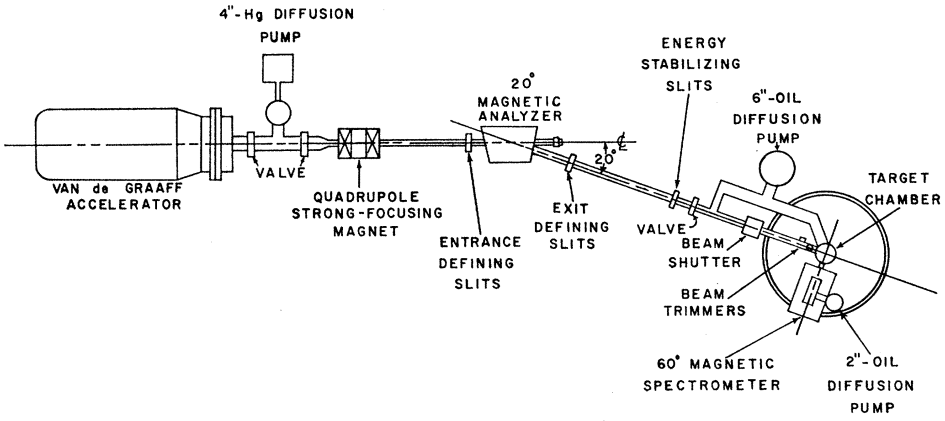

FIG. 1. Experimental arrangement.

penetration depth was found when the proton scattering took place immediately after ion bombardment as was found when the proton scattering was delayed by as much as 3 days.

The charge incident upon the target during the ion bombardment and proton scattering was measured with a current integrator. A beam shutter was used to interrupt the incident proton beam after a predetermined amount of charge had been deposited on the target. The elastically scattered protons were analyzed in momentum with a double-focusing, uniform-field, reaction-product magnet of nominal momentum resolution $p/\Delta p$ of 400. The spectrometer was calibrated against the 20° magnetic-analyzer scale by observing protons elastically scattered from known targets at a laboratory angle of 90°. The magnetic field in the analyzer and in the spectrometer were measured with NMR gaussmeters. A solid-state detector was mounted in the focal plane of the spectrometer to detect the scattered protons. The vacuum in the scattering chamber was always maintained at 1.0 to 2.0×10^{-6} mm Hg.

Thick targets of research-grade Be were obtained from Brush Beryllium Co., Cleveland, Ohio; aluminum targets of >99.8% purity were obtained from United Mineral and Chemical Corp., New York; targets of >99.9% purity of V were obtained from A. D. MacKay, New York, N.Y.; and Ni and Cu targets of >99.9% purity were obtained from the Chromium Corp. of America, Waterbury, Conn. The carbon targets were made from battery electrodes. The elastic scattering of protons from these carbon targets indicated that their purity was >99.0%. The Be, Al, and V targets were mechanically polished to a mirror finish using procedures recommended for preparing metallurgical specimens by Buehler, Ltd. The Ni and Cu targets were received with a high polish from the manufacturer and were further polished and cleaned with polishing alumina of 0.05-μ size. The targets were always transferred to the scattering chamber immediately after polishing.

III. ANALYSIS OF EXPERIMENTAL DATA

The method of analysis is described in a previous paper[5]; therefore, only a brief description of the method will be given here. The present method differs from the earlier method in that the incident proton energy E_{10} is kept fixed, while the current in the 60° spectrometer is varied manually and monotonically to discover those scattered proton energies E_{20} for which protons are detected in the spectrometer. A typical momentum profile is given in Fig. 2, where the number of protons detected in the spectrometer is plotted as a function of the scattered-proton energy E_{20}. The C and O peaks are identified from the scattering geometry and arise from surface contamination of the target. The continuum at energies less than 1117.6 keV is due to scattering of protons from Be; the Be surface is at 1117.6 keV and the points corresponding to lower energies are due to protons scattered from Be atoms beneath the surface of the target. After bombardment of the Be target with 1.0-MeV Xe^+ ions, a broad distribution in the profile appears at scattered proton energy $E_{20}=1337.6$ keV. This peak is identified as due to xenon. From the scattering geometry and kinematics one can show that if the xenon were on the surface it would be located at 1380.2 keV. The fact that the xenon peak lies at a lower energy indicates that the xenon has penetrated the outer layers of the target and that the protons lose energy in penetrating these outer layers to reach the xenon. Once the energy E_{20}' corresponding to the maximum of the xenon peak is known, the range can be calculated from

$$t(\mathrm{g/cm^2}) \equiv \rho_2 S = \frac{(\alpha E_{10} - E_{20}')\, M_2 \cos\theta_1}{[\alpha\epsilon_p(E_p^{(1)}) + (\cos\theta_1/\cos\theta_2)\,\epsilon_p(E_p^{(2)})]N_0}, \quad (1)$$

where M_2 is the target-atom mass, ρ_2 is the density of the target in g/cm^3, S is the penetration depth in cm of the Xe beneath the surface, $\theta_1(\approx 45°)$ is the angle between the incident proton beam E_{10} and the normal to the target, $\theta_2(\approx 45°)$ is the angle between the scat-

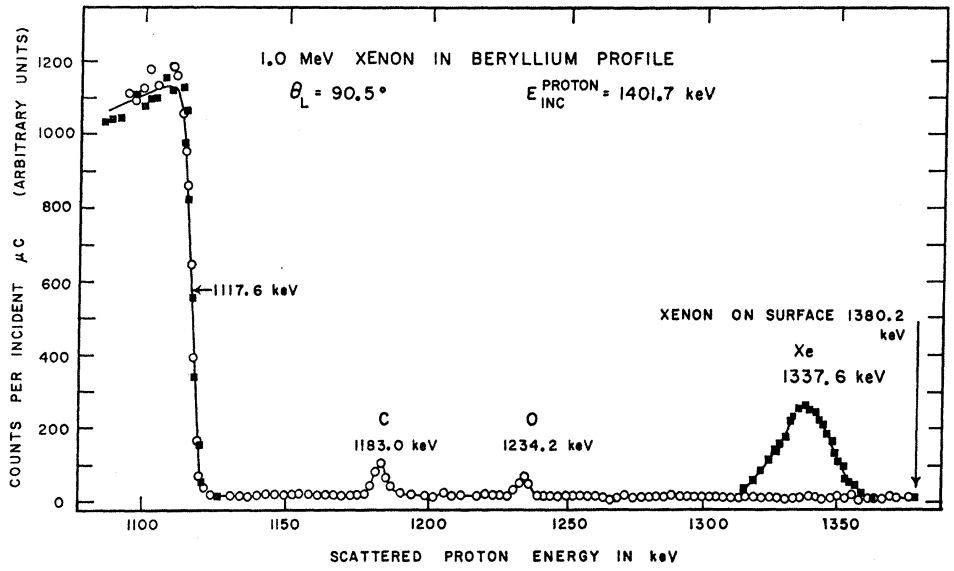

FIG. 2. The number of protons scattered as a function of scattered-proton energy at a laboratory angle of 90.5° at proton bombarding energy 1401.7 keV. The curve through the open circles was measured before, and the curve through the squares after, the Be target has been bombarded with 900 μC/cm^2 of 1.0-MeV Xe^+ ions. If the Xe were on the surface, the scattering geometry dictates that it would be at 1380.2 keV; however, the maximum of the Xe peak is at 1337.6 keV, thereby indicating that the Xe is located beneath the surface of the target.

tered proton beam E_{20} and the normal to the target,

$$\alpha^{1/2}=\frac{M_1\cos\theta_L}{M_1+M_2'}+\left[\left(\frac{M_1\cos\theta_L}{M_1+M_2'}\right)^2+\frac{M_2'-M_1}{M_2'+M_1}\right]^{1/2}, \quad (2)$$

M_1 is the mass of the proton, M_2' is the mass of the xenon ion, θ_L is the laboratory scattering angle, $\epsilon_p=-dE/(Ndx)$ is the atomic stopping cross section for protons in the target material, N is the number of target atoms per unit volume, N_0 is Avogadro's number, $E_p^{(1)}=\frac{1}{2}(E_{10}+E_{1S})$, $E_p^{(2)}=\frac{1}{2}(E_{20}+E_{2S})$, E_{1S} is the incident proton energy at a distance S beneath the surface, and $E_{2S}=\alpha E_{1S}$. The proton-stopping cross sections are known in the energy range covered by this experiment for all targets except V. The accuracy of the proton stopping cross sections is as follows[8]: Be: ±3%; C: ±4% Al: ±5%; Ni and Cu: ±8%. The V has been measured in the present experiment to an accuracy of ±4%.

IV. PROTON-STOPPING CROSS SECTION OF VANADIUM

The measurement technique is due to Warters[9] and consists of evaporating a thin uniform layer of V of known surface area on a backing of high atomic number, such as Ta. The sample is weighed carefully with a precision microbalance before and after vacuum deposition to determine the thickness x of the layer. By elastically scattering protons from the Ta before and after deposition of the V, one can determine the proton-stopping cross section according to Warters as

$$\epsilon_p=-N^{-1}\frac{dE}{dx}$$
$$=\epsilon_p\left(\frac{E_{2B}+E_{20}}{\alpha_{Ta}+1}+\frac{E_{2B}-E_{20}}{2(\alpha_{Ta}+1)}\frac{\eta'-\alpha_{Ta}}{\eta'+\alpha_{Ta}}\right)$$
$$=(E_{2B}-E_{20})/B,$$

where $E_{2B}=\alpha_{Ta}E_{10}$=scattered proton energy from the surface of a clean Ta target, E_{20}=scattered proton energy from Ta after the protons have first penetrated the V layer, $B=Nx(\alpha_{Ta}+1)/\cos\theta_1$, $\eta'\equiv\epsilon_p^V(E_{20})/\epsilon_p^V(E_{10})$ is the ratio of the proton-stopping cross section of V at E_{20} to that evaluated at E_{10}, α_{Ta} is found from (2), and θ_1 is the same angle as mentioned in Eq. (1).

Because the proton-bombarding energies E_{10} in the Xe in V measurements were kept in the vicinity of 2 MeV, only three measurements of the proton-stopping cross sections were made. The probable error in these absolute measurements is estimated to be less than 4%. This assignment is based on the following sources of error: (1) uniformity of the V layer: ±3%; (2) area of V layer: ±0.5%; (3) weight measurement: ±1%; (4) uncertainty in energy difference $E_{2B}-E_{20}$: ±1.6%; (5) uncertainty in θ_1: ±0.4%. The total probable error calculated from the square root of the sum of these independent errors is ±3.64%. The values of ϵ_p are

proton energy (keV)	$\epsilon_p=-dE/(Ndx)$ (10^{-15} eV cm^2)
559.2	17.7
1776.1	8.33
1984.1	7.84

The reason for the lower-energy measurement is that

[8] W. Whaling, in *Handbuch der Physik*, edited by S. Flügge (Springer–Verlag, Berlin, 1958), Vol. 34, p. 193.
[9] W. D. Warters, Ph.D. thesis, California Institute of Technology, 1953 (unpublished).

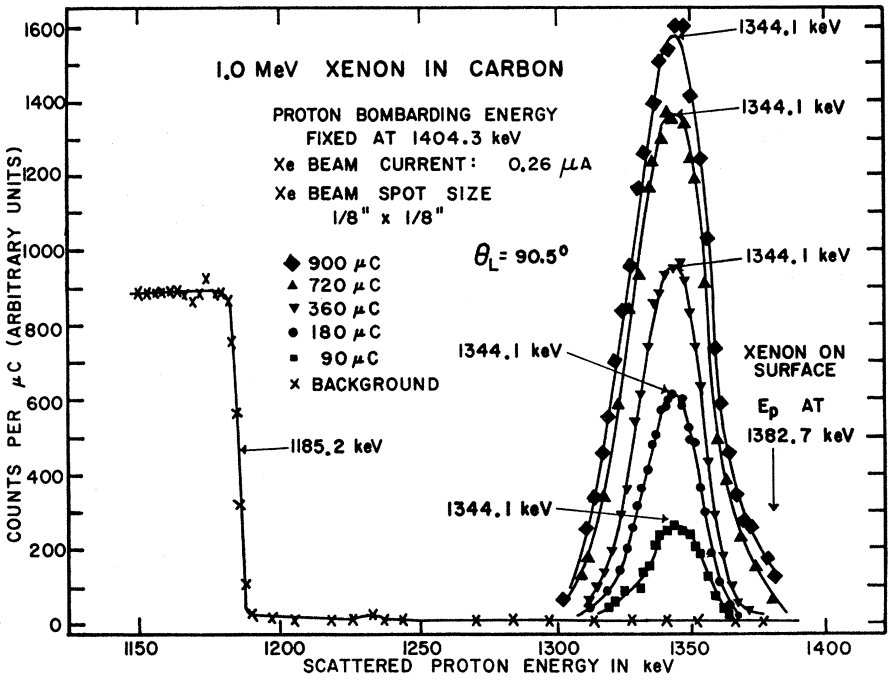

FIG. 3. Experimental test of saturation of a carbon target with different concentration of 1.0-MeV Xe^+ ions. The concentrations vary from 90–900 μC (corresponding to 900–9000 $\mu C/cm^2$) with the maximum of the peak indicated in each instance to be at 1344.1 keV. The beam current density was 2.6 $\mu A/cm^2$.

Bader *et al.*[10] had previously found that the proton-stopping cross section in V at 500 keV was 18.5×10^{-15} eV cm^2 and at 600 keV was 16.6×10^{-15} eV cm^2, and it was desirable to compare our results to theirs. The present measurement at 559.2 keV agrees quite well with these two previous measurements. It should also be pointed out that the present measurements at 1776.1 and 1984.1 keV agree quite well with the Bethe-Bloch formula using as an estimate for the mean ionization potential I the value given by Seb.[11] Seb suggests that the approximation $I=kZ$ is inaccurate and that a better estimate is given by $I=kZ^n$, with $k=17$ and $n=0.86$. The agreement between the experimental results and Seb's prediction is very good.

V. PHENOMENA AFFECTING RANGE MEASUREMENTS

A. Effect of Embedded Atoms

It is essential to determine whether atoms deposited at the beginning of the ion bombardment affect the range of ions which subsequently penetrate the target (effect of saturation). Five different spots on a carbon target were bombarded with 1-MeV Xe^+ ions in concentrations ranging from 900 to 9000 $\mu C/cm^2$. Figure 3 shows the results of the scattering of 1404.3-keV protons. Only one background of the carbon is included in the figure, but the proton scattering from the carbon surface (midpoint of the carbon step) was carefully run on each xenon spot with the result that the midpoint of the carbon step remained precisely at 1185.2 keV on all five proton scattering runs. It is immediately apparent from this figure that the location of the peak is independent of the amount of ion deposited, at least for concentrations between 900 and 9000 $\mu C/cm^2$. One may conclude that saturation either has not yet set in or has already occurred in the target. The former conclusion appears to be the correct one, since the 90 μC profile gives no evidence of the presence of the xenon from the surface at 1382.7 keV down to about 1364 keV (roughly half of the actual penetration depth). If one normalizes the scattering peak of the 900-μC bombardment to that of the 90-μC bombardment (i.e., to 200 counts), then the corresponding count rate at 1382.7 keV (i.e., at the surface) is only about 19 counts. The fact that there is a finite count rate at the surface for this greater concentration of xenon bombardment indicates the presence of some xenon on the surface, as expected when the stopping of xenon in xenon begins to occur. These results show that although saturation is taking place in the 9000-$\mu C/cm^2$ bombardment, the saturation has no effect on the measured range since the maximum of the peak occurs at precisely the same energy as does the lower-concentration bombardment. It was mentioned previously that the ion-beam charge density was 900 $\mu C/cm^2$ for the xenon range measurements, 5000 $\mu C/cm^2$ for the Kr range measurements, and 9000 $\mu C/cm^2$ for the argon range measurements. These three concentrations lie within the limits of the concentrations used in this

[10] M. Bader, R. E. Pixley, F. S. Mozer, and W. Whaling, Phys. Rev. **103**, 32 (1956).
[11] Do In Seb, Zh. Eksperim. i Teor. Fiz. **43**, 121 (1962) [English transl.: Soviet Phys.—JETP **16**, 87 (1963)].

test, so that it is concluded that throughout the range measurements the presence of the embedded atoms does not alter the range of those ions which hit the target at a later time during the bombardment. It is also concluded that it is safe to neglect the proton stopping by the embedded atoms and to use only ϵ_p for the target atom when calculating the ion ranges by Eq. (1).

It should be mentioned that Domeij in a recent paper[12] measured the channeling of α particles emitted from Rn^{222} embedded in a W single crystal. The Rn^{222} ions were injected into the crystal at energies between 5 and 450 keV. Domeij states that saturation effects should be present if more than 10^{14} atoms/cm^2 are injected into the crystal. The beam densities of the present experiment exceed this amount by one to two orders of magnitude, yet there does not seem to be any saturation effect as discussed above. It is not clear that the beam densities which produce saturation in the two experiments can be directly compared.

Barker and Phillips,[13] in measuring the ranges of N in Ni and Ag from 0.4 to 2.5 MeV by means of the $N^{15}(p, \alpha\gamma)C^{12}$ reaction, used concentrations of injection of about 10^{16} atoms, which corresponds roughly to the maximum concentration (9000 μC/cm^2) used in the present experiment.

B. Proton Energy and Scattering Geometry

The proton bombarding energies used in determining the ranges varied from 800 keV to 2.1 MeV. The laboratory scattering angle was fixed at 90.0° or 90.5° throughout all the measurements. The choice of a particular proton energy was dictated by experimental conditions. It is desirable to keep the ion peak to the right of the target step in the profile where the background is negligible. If the ion peak lies on top of the step, uncertainties in locating the maximum of the peak are encountered in subtracting two relatively large counting rates from each other to obtain a relatively small counting rate. For measurements such as Xe in V, Ni, and Cu it was essential to use a high proton energy such as 2.1 MeV to keep the Xe off the target step, and even then it was not possible for the xenon-in-copper measurement to use a higher energy than 1.5 MeV for the xenon ion before running into the copper step. It is also desirable to keep the ion peak away from the surface peaks such as C and O, and this could easily be accomplished by a judicious choice of proton energy E_{10}. In order to test the consistency of the method, however, different proton energies E_{10} were used on those range measurements, where the ion peak was well displaced from the target step (such as Xe or Kr in C or Be). All these tests, utilizing different proton-bombardment energies, yielded the same result in the range measurement. The consistency of the scattering geometry is implied since the 500-keV measurements at Caltech[5] were run at a laboratory scattering angle of 130°, whereas the present measurements were at 90°. Comparison was made in the Kr and Ar measurements at 500 keV with good agreement between the two sets of data being obtained.

C. Localized Heating of the Target

A test was also made to insure that no localized heating of the target from the ion beam or the proton beam was occurring which could affect the range. A special water-cooled target holder was prepared so that the target could be held in thermal contact with a copper heat sink which was water-cooled to about 40°F. An ion-beam current density of 37 μA/cm^2 (approximately $7\frac{1}{2}$ times as high as any ion current density actually used in the range measurements) was obtained for a 1.5-MeV Kr beam, and the range in Al was measured with water-cooling of the target and without water-cooling. The proton-beam current density was kept at about 12 μA/cm^2, both in this test and in the actual range measurements. The same experiment was repeated at ion-beam current density 14 μA/cm^2 with cooling and without cooling, and both the range and range straggling remained unchanged in all four cases. Since the actual ion-beam current densities were 5 μA/cm^2 or less in the range measurements and the proton current density was $\sim$12 μA/cm^2, it was concluded that no severe localized heating of the target was occurring which could influence either the range or the range straggling.

D. Effect of Proton Bombardment

An independent test of the effect of the proton beam was also run. This test involved the use of a 16-in. scattering chamber and a surface-barrier detector cooled to dry-ice temperatures. Although the resolution of this system is not as good as the resolution of the 60° magnetic-spectrometer system, the system does enable one to make a complete display of the entire spectrum on a multichannel pulse-height analyzer with a minimum of deposition of proton beam on the target. An Al target, which had been previously bombarded by xenon ions was bombarded 35 times in discrete steps of 3000 μC/cm^2 of proton beam with the proton scattering being displayed on the analyzer after each 3000 μC/cm^2 of deposition. The profiles indicated in all cases from 3000 to 105 000 μC/cm^2 that neither the peak had shifted nor had the full width at half-maximum (FWHM) changed. Since none of the proton bombardments reached 105 000 μC/cm^2 of proton beam deposited, it is reasonable to assume that the amount of proton beam deposited into the target had no effect on the range and range-straggling measurements.

E. Polycrystalline Nature of Targets

If direct comparison is to be made between the present results and Lindhard's (random) theory, care must

[12] Bo Domeij, Arkiv Fysik **32**, 179 (1966).
[13] P. H. Barker and W. R. Phillips, Proc. Phys. Soc. (London) **86**, 379 (1965).

be taken to insure that all the targets have a distinct polycrystalline or amorphous structure. Back-reflection x-ray photographs were run on each target used in the range measurements and all targets showed a definite polycrystalline structure. X-ray diffractometer patterns were also run on each target to determine the physical size of each particle crystal making up the polycrystalline metal. In every case except Ni and Cu the minimum Xe range (corresponding to 500 keV) was several times larger than the particle size. For Cu and Ni the particle size was about the same dimension as the minimum xenon range. Because the proton-beam size and ion-beam size are several thousand times larger than any of the particle domains constituting the crystal, the moving ions should still encounter essentially a random array of target atoms, since the proton scattering will display the average effect of the several thousand orientations.

F. Effect of Surface Contamination

The accumulation of contamination on the target surface during ion and proton bombardment affects both ion and proton energies and thus affects the ranges calculated from these energies. The vacuum in the target chamber throughout all the measurements was kept in the vicinity of $1\text{–}2\times10^{-6}$ mm Hg by means of an efficient optically dense liquid-nitrogen trap at the junction of the target chamber and the 6-in. pump. Surface layers are detected by a shift to lower energy in the midpoint of the target-atom step in the profile. The position of the midpoint of this step was measured immediately following each ion bombardment and also after the embedded-atom peak was run in the profile. No detectable shift was observed in any of these measurements, and we are therefore neglecting surface-contamination corrections as a factor in the present measurements.

VI. RANGE STRAGGLING

The range-straggling parameter Ω is defined as the FWHM of the distribution of embedded atoms in the target. The procedure for calculating the range straggling is described in a previous paper,[5] but must be modified slightly since the incident-proton energy is kept fixed in the present experiment, whereas the scattered-proton energy was kept fixed in the previous experiment. The straggling Ω is given as $\Omega=(\rho dR/dE_{20})\delta$, where $\delta^2=\delta E_{20}^2-\delta_{\text{inst}}^2-\delta_p^2$. δE_{20} is the FWHM on the embedded-atom peak in the profile, δ_{inst} includes all contributions from finite instrumental resolution, and δ_p is the proton energy straggling.

The instrumental resolution δ_{inst} may be written as[14]

$$\delta_{\text{inst}}^2=\tfrac{2}{3}(\ln 2)[E_{10}(\partial\alpha/\partial\theta_L)\Delta\theta_L]^2+\delta_0^2,$$

where the first term is due to the variation of scattered-proton energy with angle $\Delta\theta_L$ over the aperture of the spectrometer, and where δ_0 is constant and includes all other sources of finite resolution such as finite beam-spot size, inhomogeneity of incident proton beam, and finite collector-slit width. The above equation allows for the variation of δ_{inst} with the mass of the scattering atom and may be evaluated with the aid of Eq. (2). δ_{inst} can be measured directly from the width ΔE_{20} of the target step in the profile for a particular M_2 by the relation $\delta_{\text{inst}}^2=4\ln 2(\Delta E_{20})^2/\pi$, and δ_{inst} can then be calculated for any other mass M_2.

The proton straggling δ_p is given as

$$\delta_p^2=4(2\ln 2)4\pi e^4NZ_2S[\alpha^2/\cos\theta_1+1/\cos\theta_2],$$

where Bohr's[1] expression $\sigma_B^2=4\pi e^4NZ_2R$ is used for the mean-square energy deviation of an initially monoenergetic proton beam after passing through an absorber of thickness R and atomic number Z_2 containing N atoms/cm^3. For some of the lower-energy-range measurements the ions stop near the surface, so that S for the lower half-maximum differs appreciably from S at the upper half-maximum. For these cases, δ_p is evaluated at both points and the correction to each half of the observed distribution is calculated separately.

VII. ACCURACY

The sources of experimental error are listed in Table I, where the first column gives the parameter entering the range calculation, the second column gives the probable error in percent for each parameter, and the final column gives the contribution to the probable error in the range. When two numbers appear in the middle and last column, the first refers to the 500-keV ions and the last to the measurement with the least percent of error. The least percent of error in most instances was associated with the 2-MeV-ion measurements, and the errors of the intermediate ranges between 500 keV and 2 MeV generally decreased with ion energy. The 500-keV measurements have larger uncertainties than the higher-energy measurements because the embedded atoms are close to the surface. The table is for Kr in Al, but these results are typical of all the measurements. The principal sources of error are: location of ion peak in profile, drift in 60° spectrometer, and uncertainty in proton stopping cross section. The limits on the accuracy of the measurements expressed in percent as a probable error are: Ar in Be: 4.8–3.2%; Ar in C: 6.0–4.4%; Kr in Be: 8.1–3.4%; Kr in C: 10.1–5.4%; Kr in Al: 7.5–5.7%; Xe in Be: 8.9–3.8%; Xe in C: 8.9–5.1%; Xe in Al: 8.7–6.1%; Xe in V: 8.6–5.7%; Xe in Ni: 10.7–8.8%; and Xe in Cu: 11.4–8.9%. In some cases, such as Xe in Ni and Cu, the individual range measurements were found to vary from 13–21%. The reason for this large uncertainty is that when a proton bombarding energy of 2.1 MeV was used, a very small uncertainty in the

[14] The equation for δ_{inst} in Ref. 5 is incorrect and should be

$$\delta_{\text{inst}}^2=\tfrac{2}{3}(\ln 2)\{E_{20}[\partial(\alpha^{-1})/\partial\theta_L]\Delta\theta_L\}^2+\delta_0^2.$$

The correct equation was used in calculating the range straggling reported in Ref. 5.

TABLE I. Experimental accuracy of the range measurements on Kr in Al.

	Source of error	Probable error (%)	Probable error in range from this source (%)
E_{10}	Drift of 20° magnetic-analyzer setting	±0.15	±0.14
E_{10}	Calibration of 20° magnet	0.15	0.14–0
E_{20}	Drift in 60° magnetic-spectrometer setting	0.03	3.8–1.0
E_{20}	Determination of midpoint of Al step in profile	0.015	2.3–0.6
E_{20}	Location of ion peak in profile	0.02–0.085	3.0–3.9
θ_1	Uncertainty in θ_1	0.44	0.15
θ_2	Uncertainty in θ_2	0.44	0.20
θ_L	Uncertainty in θ_L	0.17	1.0–0.3
ϵ_p	Uncertainty in proton-stopping cross sections	5	5

Root-mean-square probable error: ±7.5–5.7%

location of the ion peak or the midpoint of the step would result in a large uncertainty in the range. For these cases the random errors were minimized by repeating these measurements in some instances by as many as six times. Because the proton-stopping cross section in Ni and Cu is known at 2.0 MeV to only ±8.0%, the present measurements in Ni and Cu can be no more accurate than ±8%. The proton-stopping cross sections could have been measured to ±4% in Ni and Cu as in V, but the ranges would have improved in accuracy from 11.4–8.4%; the additional effort was not considered worthwhile.

VIII. RESULTS

The ranges and range straggling in $\mu g/cm^2$ as measured in this experiment are given in Table II. The Ar measurements in Be and C indicate a dE/dx increasing with ion energy. The straggling measurements are excluded in the table for the C targets because of the porous nature of the C. The V, Ni, and Cu straggling measurements were excluded because the embedded-atom peak overlapped the step in the profile, and a quantitative assignment of range straggling would have been difficult because of large extrapolations in the data. The maximum of the peak was clearly resolved from the step in these latter measurements, so that no ambiguity was present in the range itself.

In order to make comparison to the theory,[4] one must express the range R and the energy E in Lindhard's dimensionless units ρ and ϵ, defined as

$$\rho = RNM_2[4\pi a^2 M_1/(M_1+M_2)^2],$$

$$\epsilon = [EaM_2/Z_1Z_2e^2(M_1+M_2)],$$

where the screening parameter a is given by $a=a_0\times 0.8853(Z_1^{2/3}+Z_2^{2/3})^{-1/2}$, Z_1 and Z_2 are the atomic numbers of the incident ion and target atom, respectively, $a_0=5.29\times10^{-9}$ cm, and e is the electron's charge. A dimensionless rate of energy loss $d\epsilon/d\rho$ is found by adding linearly the energy loss due to nuclear elastic collisions $(d\epsilon/d\rho)_{\text{nucl}}$ to the energy loss by electronic excitation and ionization, which the theory predicts to be

$$(d\epsilon/d\rho)_{\text{elec}} = k\epsilon^{1/2} = \xi_e \frac{0.0793 Z_1^{1/2} Z_2^{1/2} (A_1+A_2)^{3/2}}{(Z_1^{2/3}+Z_2^{2/3})^{3/4} A_1^{3/2} A_2^{1/2}} \epsilon^{1/2}, \quad (3)$$

with $\xi_e \approx Z_1^{1/6}$. The energy loss due to nuclear collisions is based on a Thomas-Fermi picture and approaches Bohr's expression[1] for nuclear elastic stopping in an unscreened Coulomb field expressed in ρ-ϵ units as $(d\epsilon/d\rho)$ (unscreened nuclear) $= (1/2\epsilon)\ \ln 2\epsilon$. Lindhard and co-workers only plot ρ-ϵ curves for particular values of the electronic stopping constant k, so that in order to make a more direct comparison between theory and experiment, we fitted a curve to their $(d\epsilon/d\rho)_{\text{nucl}}$, which is plotted in their paper up to values of $\epsilon=16$, and we used Bohr's $(d\epsilon/d\rho)_{\text{nucl}} = (1/2\epsilon)\ \ln 2\epsilon$ for ϵ values greater than 29. For $16<\epsilon<29$ we joined the two extrapolated curves smoothly. The electronic stopping $(d\epsilon/d\rho)_{\text{elec}} = k\epsilon^{1/2}$ is added to $(d\epsilon/d\rho)_{\text{nucl}}$ to obtain a $(d\epsilon/d\rho)_{\text{tot}}$, which is then numerically integrated to get

$$\rho = \int_0^{\epsilon} d\epsilon \Big/ \left(\frac{d\epsilon}{d\rho}\right)_{\text{tot}}$$

as a function of ϵ. The k values for combinations of ions and targets in the present experiment varied from $k=0.092$ for Ar in Be to $k=0.129$ for Xe in Cu. By taking these limits on k, one can calculate from the theoretical curves the ϵ value for which electronic stopping should be equal to the nuclear stopping. (ϵ values greater than this value correspond to processes where electronic stopping is more dominant.) This ϵ value would enable one for the particular measurements to tell which process is dominating the stopping picture

TABLE II. Experimental values of the range and range straggling. The uncertainties listed are probable errors. When no uncertainty is listed, the probable error is less than 0.5%.

Ion and target	Ion energy (keV)	Range ($\mu g/cm^2$)	Range straggling ($\mu g/cm^2$)
Ar in Be	503.0	87.3±4.2	40.4±4.3
	613.0	106.5±3.7	45.4±3.3
	706.0	121.1±5.4	42.6±5.6
	804.9	137.5±5.7	44.9±6.0
	906.4	151.2±5.4	42.8±5.8
	1000.6	174.8±7.5	53.1±7.9
	1100.6	186.4±7.0	55.9±7.5
	1199.5	197.3±7.0	67.6±7.8
	1299.8	211.1±7.7	52.6±8.3
	1399.9	224.7±8.1	44.9±8.5
	1500.2	234.0±8.3	52.8±8.9
	1601.0	249.6±8.1	63.0±7.8
	1700.8	252.9±8.8	53.1±9.5
	1800.1	267.2±9.3	59.8±9.9
	1898.7	279.2±9.6	55.9±10.3
	2000.6	289.6±9.6	49.6±10.3
Ar in C	500.8	88.4±5.3	···
	606.5	102.2±5.6	···
	703.8	112.9±5.0	···
	800.2	123.9±7.0	···
	900.3	138.0±8.3	···
	999.8	152.0±8.2	···
	1100.4	171.8±11.2	···
	1200.1	181.4±10.4	···
	1300.7	191.1±10.7	···
	1400.2	200.8±11.9	···
	1500.5	217.9±13.4	···
	1599.3	230.4±11.8	···
	1699.8	236.5±12.9	···
	1799.2	244.5±12.4	···
	1900.5	254.5±14.4	···
	1999.0	271.0±14.0	···
Kr in Be	501.2	57.4±3.4	39.1±3.2
	600.7	63.7±3.9	46.6±3.0
	700.6	77.4±4.1	51.4±3.3
	801.4	93.9±5.8	50.2±4.9
	901.6	102.3±5.9	53.8±5.3
	1000.2	117.0±4.7	59.8±4.1
	1102.0	127.7±6.4	61.7±6.1
	1202.1	139.7±6.6	68.5±6.5
	1302.2	150.3±8.1	71.5±8.1
	1402.2	156.9±7.7	71.4±7.6
	1502.4	172.9±8.7	71.0±8.8
	1603.0	189.0±8.9	79.7±9.0
	1702.8	201.1±8.6	73.7±8.8
	1803.2	207.6±9.3	88.0±9.7
	1901.1	227.6±7.8	82.8±6.8
	2003.0	237.1±9.9	78.1±10.3
Kr in C	499.6	47.5±4.8	···
	599.7	59.3±5.0	···
	699.6	70.3±5.1	···
	799.5	81.0±5.7	···
	899.9	92.3±6.0	···
	999.3	108.3±6.6	···
	1099.2	116.3±6.5	···
	1199.0	125.9±8.0	···
	1298.9	138.8±9.4	···
	1398.9	148.3±8.6	···
	1498.6	160.4±9.0	···
	1598.9	169.8±9.2	···
	1698.4	179.7±10.4	···
	1798.7	189.1±10.7	···
	1898.0	198.4±11.0	···
	1998.2	206.1±11.2	···
Kr in Al	399.9	45.6±3.4	55.0±4.2
	499.8	66.4±4.8	60.6±5.7
	616.0	83.7±5.5	72.6±6.6
	718.5	96.7±6.6	79.6±7.9
	820.9	105.0±7.7	88.8±9.1
	899.5	120.0±7.5	94.2±9.3
	1026.3	138.7±8.3	108.4±10.7
	1129.0	155.8±9.4	109.9±11.7
	1231.3	168.5±10.0	124.0±13.1
	1335.8	185.5±11.5	119.6±14.0
	1498.7	206.6±11.7	155.9±15.2
	1599.5	219.9±13.6	144.9±16.5
	1698.7	237.2±14.6	149.2±17.6
	1798.5	251.9±14.5	173.5±18.4
	1898.6	261.7±15.6	158.0±18.9
	1998.6	271.3±17.7	157.3±20.7
Xe in Be	401.0	26.7±2.0	21.1±1.6
	501.2	34.5±2.5	27.9±1.9
	601.4	42.2±2.9	28.2±2.1
	701.5	52.9±4.7	33.1±3.9
	801.7	60.2±3.3	36.4±2.4
	901.5	68.5±4.5	35.1±3.8
	1002.1	74.8±4.5	41.1±3.9
	1102.3	83.9±5.9	44.4±5.6
	1202.4	90.5±5.5	45.5±5.2
	1302.6	99.4±6.1	50.2±6.0
	1402.7	108.5±5.6	54.6±4.8
	1503.0	116.3±6.1	55.1±6.1
	1603.1	123.7±5.8	56.1±5.9
	1703.3	136.1±6.7	54.3±6.7
	1803.2	143.3±6.5	58.0±6.5
	1903.6	150.9±6.4	59.0±6.6
	2003.9	162.0±6.1	46.6±6.5
Xe in C	501.2	35.6±2.9	···
	606.4	43.0±3.0	···
	701.5	47.4±4.2	···
	801.7	56.5±4.1	···
	901.9	63.0±4.4	···
	1002.0	72.3±5.3	···
	1102.3	77.8±4.5	···
	1202.4	87.8±5.2	···
	1302.5	98.6±5.0	···
	1402.8	104.6±5.3	···
	1503.0	113.8±6.9	···
	1603.0	121.1±6.2	···
	1703.2	121.8±7.0	···
	1803.6	127.4±7.9	···
	1903.8	137.4±8.2	···
	2003.7	145.8±8.4	···

TABLE II. *Continued.*

Ion and target	Ion energy (keV)	Range (μg/cm)^2	Range straggling (μg/cm^2)
Xe in Al	501.0	41.4±3.3	47.2±3.8
	601.4	47.4±4.0	56.0±4.7
	701.6	61.1±5.3	53.8±6.1
	801.8	68.4±4.2	63.3±4.6
	901.8	75.6±6.0	69.3±7.2
	1002.0	85.8±5.9	69.4±6.4
	1102.2	96.8±6.8	77.6±8.2
	1202.4	105.1±8.9	87.7±10.3
	1302.5	113.8±8.7	94.0±10.4
	1402.7	125.5±9.1	97.0±10.9
	1502.9	140.4±10.0	93.9±11.7
	1603.3	146.0±10.2	91.4±11.8
	1703.5	152.2±11.8	114.1±13.7
	1803.4	165.5±12.2	113.1±14.2
	1903.7	175.1±14.0	112.6±15.9
	2003.9	187.4±14.4	122.4±16.3
Xe in V	501.1	46.3±3.4	···
	751.6	72.9±5.3	···
	1002.1	103.3±6.8	···
	1252.5	125.1±7.0	···
	1502.9	153.9±8.7	···
	1753.3	179.4±15.5	···
Xe in Ni	501.2	42.5±4.4	···
	751.6	57.4±6.1	···
	1002.1	77.5±7.9	···
	1252.5	105.1±11.2	···
	1502.8	130.3±11.5	···
Xe in Cu	501.2	48.2±5.5	···
	751.5	70.2±7.8	···
	1002.4	89.3±8.6	···
	1252.6	105.0±10.9	···
	1503.0	117.6±10.5	···

according to the theory. The ϵ value for $k=0.092$ (Ar in Be) for equal electronic and nuclear stopping is $\sim$4.6 and is $\epsilon\sim$3.2 for $k=0.129$ (Xe in Cu). The ϵ values for the Xe measurements varied from $\sim$0.69 to 4.7, thus indicating that nuclear stopping should predominate except for the highest-energy Xe measurements in Be and C, where the electronic stopping is slightly greater than the nuclear stopping. For the Kr measurements, ϵ goes from 1.7 to 12.0, so that electronic stopping should be greater than nuclear stoping over most of the energy interval. For the Ar measurements, ϵ varied from 10.9 to 54.3, so that electronic stopping should essentially dominate the stopping process according to the theory.

Our experimental results in ρ-ϵ units are plotted in Figs. 4–6. In Fig. 4 the short-dash curve is the theoret-

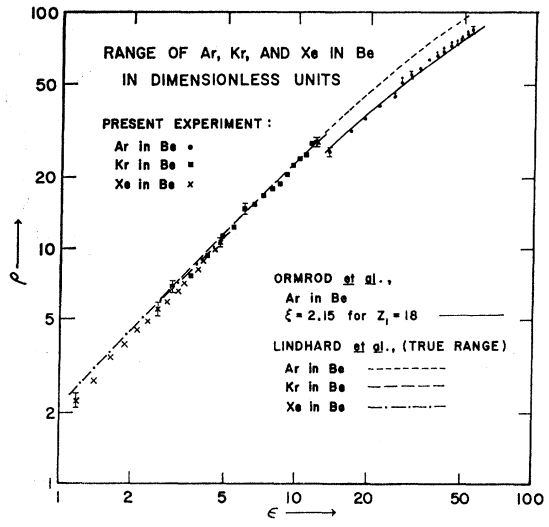

FIG. 4. Experimental values of ρ as a function of ϵ for Ar, Kr, and Xe in Be. The short-dash curve is the theoretical prediction (Ref. 4) for Ar in Be, the long-dash curve is for Kr in Be, and the dot-dash curve is for Xe in Be. The circles are the measurements on Ar in Be, the squares are the measurements on Kr in Be, and the x's are the measurements on Xe in Be. The arrows are projection corrections and the error bars are probable errors in the measurements. The solid curve is the theoretical prediction for Ar in Be using Ormrod, MacDonald, and Duckworth's measured value $\xi_e=2.15$ (see text).

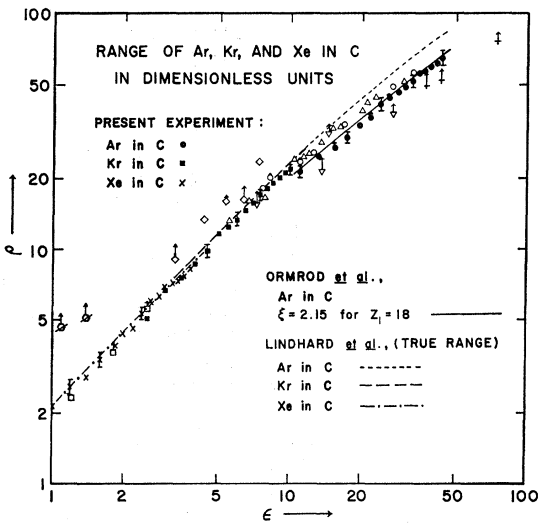

FIG. 5. Experimental values of ρ as a function of ϵ for Ar, Kr, and Xe in C. The diamonds are the measurements of Ga in gases by Bryde *et al.* (Ref. 23), the hexagons with diagonal bars are measurements of At in Ag by Leachman and Atterling (Ref. 22), the open squares are Kr^{85} in Al by Davies *et al.* (Ref. 15), the open circles are Tb^{149} in Al by Winsberg and Alexander (Ref. 19), open triangles are Tb^{149} in Al by Alexander and Sisson (Ref. 20), inverted open triangles are Ne and N in C by Powers and Whaling (Ref. 5), and crosses (+) are Ne and Na in Al by Poskanzer (Ref. 21). Projection corrections are indicated by vertical arrows.

ical prediction for Ar in Be, the long-dash curve for for Kr in Be, and the dot-dash curve is for Xe in Be. The experimental measurements are projected ranges along the direction perpendicular to the target surface; the vertical arrows on the Ar in Be measurements are the corrections of projected ranges to true ranges based on the theory. These corrections for Xe and Kr in Be are negligible. The Xe in Be measurements are lower than the theory by 9% at lower energies, but agree with the theory at higher energies.

The Xe in Be measurements at 400 and 500 keV are lower than the Caltech measurements[5] at these energies. The 500-keV measurement at Baylor was repeated four times with a result that was consistently lower than the Caltech measurement, and with each repeated measurement being within 8% of the mean value. In order to eliminate systematic errors as an explanation of this discrepancy, we decided to repeat our Kr in Al measurements which were run three months before the measurements on Xe in Be. Our range of Kr in Al at 616.0 keV of 83.7 ± 5.5 $\mu g/cm^2$ is consistent with the value 79.5 $\mu g/cm^2$ for Kr^{85} in Al at 600 keV obtained by Davies *et al.*[15] One month after all the measurements reported in the present paper had been made we twice repeated the measurements on Kr in Al at 500 keV and at 1.0 MeV and obtained the same results as before. These results eliminated the possibility of a systematic error being introduced between the original measurements on Kr in Al and the measurements on Xe in Be, and further checked the consistency and reproducibility of the measurements. We also twice repeated the 500 keV through 1.0 MeV measurements on Xe in Be and obtained the same results as before. The Caltech measurements of Xe in Be were never repeated for consistency, and we therefore conclude that the Baylor measurements are more accurate.

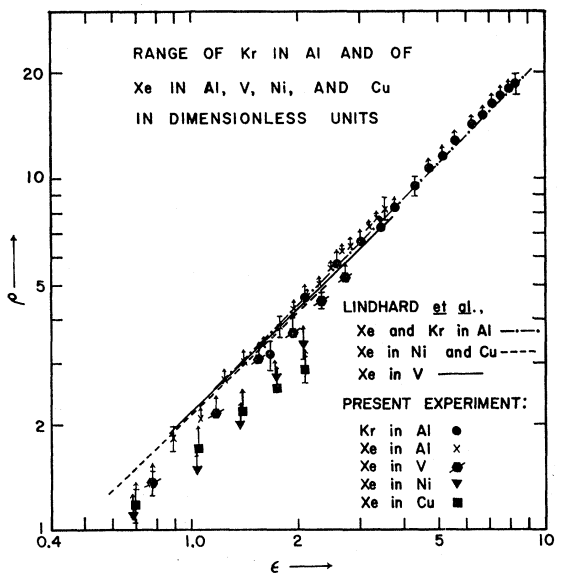

FIG. 6. Experimental values of ρ as a function of ϵ for Kr in Al and of Xe in Al, V, Ni, and Cu. Projection corrections are indicated by vertical arrows.

[15] J. A. Davies, B. Domeij, and J. Uhler, Arkiv Fysik **24**, 377 (1963).

The Kr in Be measurements in Fig. 4 are in excellent agreement with the theory over the entire energy region. The measurements on Ar in Be are consistently lower from 15 to 18% than the theory even after projection corrections have been made. Recent experiments by Ormrod, MacDonald, and Duckworth[16] indicate a periodic dependence of the electronic stopping with the atomic number of the incident ion. In particular, their results indicate that with argon as the projectile, ξ_e should be 2.15 rather than $Z_1^{1/6}=1.62$, as given by the theory. We have taken $\xi_e=2.15$, calculated ρ, and plotted the result as the solid curve in Fig. 4. The agreement between our results and the theory with Ormrod, MacDonald, and Duckworth's value of ξ_e is quite good.

Figure 5 gives the results for Ar, Kr, and Xe in C. The short-dash curve is the theoretical estimate for Ar in C, the long-dash curve is for Kr in C, and the dot-dash curve is for Xe in C. The closed circles are the experimental Ar in C measurements and are lower than the theory with $\xi_e=Z_1^{1/6}$ by 10–18% after projection corrections have been made. The solid curve represents the theory with Ormrod, MacDonald, and Duckworth's correction of $\xi_e=2.15$ and is seen to be in excellent agreement with the experimental results. The solid squares are the measurements on Kr in C and are in excellent agreement with the theory of Lindhard *et al.* over the entire energy region 0.5–2.0 MeV. The measurements on Xe in C (represented by x's) are also in excellent agreement with the theory.

The measurements of other experiments are included in Fig. 5. In selecting other measurements, we have restricted consideration to combinations of ions and targets that yield $k\sim0.09$–0.12. The theory, of course, is dependent upon the k value, and we thought it would be misleading to compare theory and experiment including measurements such as those of Barker and Phillips[13] on N^{15} of 0.4–2.5 MeV in Ni and Ag ($k=0.32$ and 0.54, respectively); of Phillips and Read[17] on N^{15} of 0.4–6.4 MeV in Au ($k=0.96$); and of Panontin *et al.*[18] on C^{11} of 0.67–1.64 MeV in Al ($k=0.22$). The open squares at $\epsilon=1.21$, 1.79, and 2.50 are the 296–, 430-, and 600-keV Kr^{85} measurements in Al ($k=0.11$) by Davies *et al.*[15] and are in excellent agreement with the present measurements. The open inverted triangles

[16] J. H. Ormrod, J. R. MacDonald, and H. E. Duckworth, Can. J. Phys. **43**, 275 (1965); J. H. Ormrod and H. E. Duckworth, *ibid.* **41**, 1424 (1963).

[17] W. R. Phillips and F. H. Read, Proc. Phys. Soc. (London) **81**, 1 (1963).

[18] J. A. Panontin, L. L. Schwartz, A. F. Stehney, E. P. Steinberg, and L. Winsberg, Phys. Rev. **140**, A151 (1965).

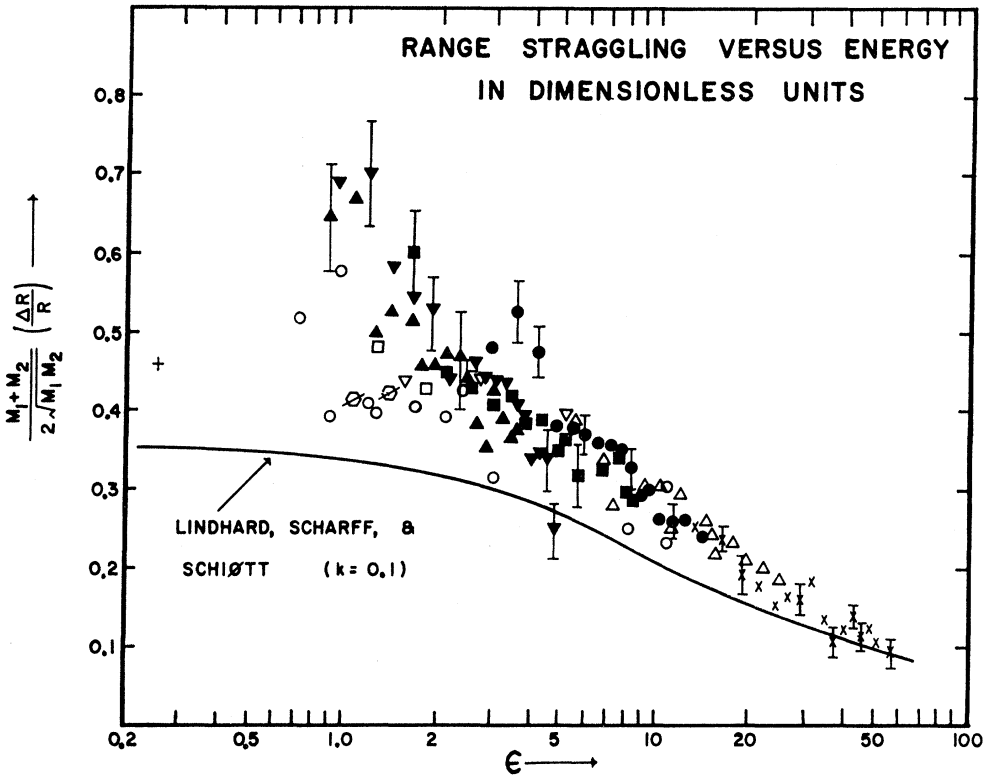

FIG. 7. Range straggling in units $(M_1+M_2)(\Delta R)/2(M_1M_2)^{1/2}R$ as a function of ϵ. The solid curve is the theoretical prediction using $k=0.1$ of Lindhard, Scharff, and Schiøtt (Ref. 4). Error bars denote probable errors of present measurements. Present measurements with symbols are: x's: Ar in Be; dark circles: Kr in Be; dark squares: Kr in Al; dark triangles: Xe in Al; dark inverted triangles: Xe in Be. Other measurements include: open triangles: Tb in Al, Alexander and Sisson (Ref. 20); open inverted triangles: Alexander and Winsberg (Ref. 19); open squares: Kr^{85} in Al, Davies *et al.* (Ref. 15); open hexagons with diagonal bars: At in Ag by Leachman and Atterling (Ref. 22); cross (+) by Bergström *et al.* (Ref. 24); open circles: Ar, Kr, and Xe in Be and Al by Powers and Whaling (Ref. 5).

are the measurements of Powers and Whaling[5] of Ne in C ($k=0.11$) and of N in C ($k=0.12$). The open circles are measurements of Winsberg and Alexander[19] of Tb^{149} in Al ($k=0.11$). The open triangles are measurements of Alexander and Sisson[20] of Tb^{149} in Al ($k=0.11$). We have included as crosses the measurements of Poskanzer[21] of Ne in Al ($k=0.149$) at $\epsilon=43.3$ ($E=1$ MeV) and of Na in Al ($k=0.145$) at $\epsilon=37.2$ ($E=1$ MeV) and at $\epsilon=74.5$ ($E=2$ MeV). The open hexagons with diagonal bars at $\epsilon=1.09$ ($E=2.2$ MeV) and at $\epsilon=1.39$ ($E=2.8$ MeV) are measurements by Leachman and Atterling[22] of At in Ag ($k=0.14$) and are considerably higher than the theoretical predictions. The open diamonds are measurements by Bryde and co-workers[23] in gases of Ga in Ar ($k=0.129$), of Ga in N_2 ($k=0.105$), and Ga in He ($k=0.097$), and are only included because the k values and ϵ values are in the region of our measurements. Their values are higher than the present measurements. Thus, the independent measurements of Davies *et al.*; Alexander, Sisson, and Winsberg; Poskanzer; and Powers and Whaling are consistent with the present results, while the measurements of Leachman and Atterling of At in Ag and of Bryde *et al.* of Ga in gases are higher than the present measurements.

Figure 6 gives the results for Kr in Al and for Xe in Al, V, Ni, and Cu. The projection corrections become more significant for these measurements because of the decreasing ratio of incident-ion mass to target-atom mass. The measurements on Kr in Al without projection correction are very close to the theoretical prediction of Lindhard *et al.*, but are 8–9% higher than the theoretical prediction after projection corrections have been made. The measurements on Xe in Al are generally in good agreement (to within 6 or 7%) with the theory after the projection corrections have been made. The measurements on Xe in V (the closed hexa-

[19] L. Winsberg and J. M. Alexander, Phys. Rev. **121**, 518 (1961).
[20] J. M. Alexander and D. H. Sisson, Phys. Rev. **128**, 2288 (1962).
[21] A. M. Poskanzer, Phys. Rev. **129**, 385 (1963).
[22] R. B. Leachman and H. Atterling, Arkiv Fysik **13**, 101 (1957).
[23] L. Bryde, N. O. Lassen, and N. O. R. Poulsen Kgl. Danske Videnskab. Selskab, Mat. Fys. Medd. **33**, No. 8 (1962).

gons with diagonal bars) agree with the theory to within 5% after projection corrections for all measurements, except the one at $\epsilon=0.77$, where the experiment is about 8% below the theory.

The measurements on Xe in Ni and Cu differ from the theory after projection corrections more than any of the other measurements. Both sets of measurements are consistently lower than the theory and differ from 11–21% for the Ni, and from 9–24% for the Cu. It was mentioned previously that each of the Ni and Cu measurements were repeated several times (some measurements as many as six times), and in all instances the experimental value after projection correction was less than the theoretical prediction.

In Fig. 7 the range-straggling parameter

$$(M_1+M_2)(\Delta R)/2(M_1M_2)^{1/2}R$$

in dimensionless units is plotted as a function of the dimensionless energy parameter ϵ. The quantity ΔR is defined as the standard deviation [the FWHM of the embedded-atom peak divided by $2(2\ln 2)^{1/2}$]. The dark points and x's refer to the present measurements, and the open circles, triangles, and squares to other measurements. The x's are the measurements on Ar in Be, the solid circles Kr in Be, the solid squares Kr in Al, the solid inverted triangles Xe in Be, and the solid triangles Xe in Al. The open triangles are the recoil measurements on Tb in Al of Alexander and Sisson.[20] The open inverted triangles are the recoil measurements of Alexander and Winsberg.[19] The open squares are the Kr^{85} measurements in Al of Davies *et al.*[15] The open hexagons with diagonal bars are the measurements on At in Ag of Leachman and Atterling.[22] The cross at $\epsilon=0.28$ is for Rn in Al as measured by Bergström *et al.*[24] The open circles are Ar, Kr, and Xe measurements[5] in Be and Al at Caltech. The straggling

$$(M_1+M_2)(\Delta R)/2(M_1M_2)^{1/2}R=0.457$$

of 600-keV Kr^{85} in Al at $\epsilon=2.51$ by Davies *et al.*[15] is in close agreement with the present measurement of

$$(M_1+M_2)(\Delta R)/2(M_1M_2)^{1/2}R=0.431$$

of 616-keV Kr in Al at $\epsilon=2.58$. The general trend of the straggling-parameter measurements is in good agreement with the measurements of Alexander, Sisson, and Winsberg. The experimental points are almost exclusively higher than the theoretical predictions, except for the measurements on Ar in Be in the region $\epsilon=$ 35–55.

[24] I. Bergström, J. A. Davies, B. Domeij, and J. Uhler, Arkiv Fysik **24**, 389 (1963).

IX. CONCLUSION

Of the 11 combinations of ions and targets used in the present experiment, seven of the 11 sets of measurements agree to within 9% with the Lindhard, Scharff, and Schiøtt theory after a projection correction has been made. The agreement appears to be best in the region where the electronic stopping is roughly equal to the nuclear stopping. The measurements on Ar in Be and C are in a velocity region where electronic stopping should predominate, and are lower than the theory using $\xi_e=Z_1^{1/6}=1.62$ by 10–18%. By replacing $Z_1^{1/6}$ by the shell-structure parameter of $\xi_e=2.15$ for Ar, as observed by Ormrod, MacDonald, and Duckworth, excellent agreement between theory and experiment is obtained. The measurements on Xe in Ni and Cu, after projection correction, are lower than the theory using $\xi_e=Z_1^{1/6}=1.94$ by 8–24%. These latter measurements are in a velocity region where the nuclear contribution to the stopping should predominate. If one uses the parameter ξ_e to adjust these Ni and Cu data, a value of ξ_e of 3.0–4.5 would be required.

ACKNOWLEDGMENTS

We are indebted to Professor Ken Hsi Wang for carefully reading the manuscript prior to publication. We would also like to express our deepest appreciation to Edwin Bates, Roy Brown, and John Griffin for many hours spent in helping to take the data, and to Roland Gooch for assisting in the $(dE/dx)_p$ measurements in V.